Radiotherapy and Oncology 132 (2019) 114–120

Contents lists available at ScienceDirect

Radiotherapy and Oncology

journal homepage: www.thegreenjournal.com

Original Article

MRI commissioning of 1.5T MR-linac systems – a multi-institutional study

Rob H.N. Tijssen [a,*], Marielle E.P. Philippens [a], Eric S. Paulson [b], Markus Glitzner [a], Brige Chugh [c], Andreas Wetscherek [d], Michael Dubec [e], Jihong Wang [f], Uulke A. van der Heide [g]

[a] Department of Radiotherapy, University Medical Center Utrecht, the Netherlands; [b] Department of Radiation Oncology, Medical College of Wisconsin, Milwaukee, United States; [c] Department of Radiation Oncology, Sunnybrook Health Sciences Centre, Toronto, Canada; [d] Joint Department of Physics, the Institute of Cancer Research and the Royal Marsden Hospital NHS Foundation Trust, London; [e] The Christie NHS Foundation Trust and the University of Manchester, UK; [f] Department of Radiation Physics, the University of Texas MD Anderson Cancer Center, Houston, United States; [g] Department of Radiation Oncology, the Netherlands Cancer Institute, Amsterdam, the Netherlands

ARTICLE INFO

Article history:
Received 17 August 2018
Received in revised form 14 November 2018
Accepted 11 December 2018
Available online 31 December 2018

Keywords:
MRI
Image-guided
MR-IGRT
Acceptance
Quality assurance
Quality control

ABSTRACT

Background: Magnetic Resonance linear accelerator (MR-linac) systems represent a new type of technology that allows for online MR-guidance for high precision radiotherapy (RT). Currently, the first MR-linac installations are being introduced clinically. Since the imaging performance of these integrated MR-linac systems is critical for their application, a thorough commissioning of the MRI performance is essential. However, guidelines on the commissioning of MR-guided RT systems are not yet defined and data on the performance of MR-linacs are not yet available.

Materials & methods: Here we describe a comprehensive commissioning protocol, which contains standard MRI performance measurements as well as dedicated hybrid tests that specifically assess the interactions between the Linac and the MRI system. The commissioning results of four MR-linac systems are presented in a multi-center study.

Results: Although the four systems showed similar performance in all the standard MRI performance tests, some differences were observed relating to the hybrid character of the systems. Field homogeneity measurements identified differences in the gantry shim configuration, which was later confirmed by the vendor.

Conclusion: Our results highlight the importance of dedicated hybrid commissioning tests and the ability to compare the machines between institutes at this very early stage of clinical introduction. Until formal guidelines and tolerances are defined the tests described in this study may be used as a practical guideline. Moreover, the multi-center results provide initial bench mark data for future MR-linac installations.

MR-guided radiotherapy systems provide high and versatile soft-tissue contrast imaging during irradiation. This increases the targeting precision particularly in parts of the body where CT provides insufficient contrast and where intra-fractional motion is considerable [1,2]. To date, two hybrid MR-linac systems for MR-guided radiotherapy are commercially available. Both are currently being introduced into the clinic. For these systems, which rely critically on adequate image guidance, a rigorous commissioning of the MRI system is essential.

Current guidelines on the commissioning of this new type of technology are lacking. While guidelines on acceptance testing and quality assurance of MRI scanners for diagnostic radiology are widely available [3,4], they do not cover the requirements that are specific to the use within radiotherapy. A number of papers that report on the use of MRI systems for treatment planning (i.e., MRI-simulation) stress the importance of measuring geometric fidelity over a large field-of-view besides general image quality [5–9]. Similar types of measurements have been performed on a hybrid MRI Cobalt-60 device [10,11]. Most papers, however, only report on individual measurements (e.g., image quality or geometric fidelity) [12] and none of these papers include the measurements needed to characterize the interactions of the MRI and a linear accelerator. The design of the MRI in the integrated MR-guided radiotherapy systems deviates from common diagnostic scanners [13–16]. The impact of these modifications on the image quality as well as the potential interactions of the Linac components with the MRI must therefore be carefully characterized.

The aim of this study is threefold: (1) design a comprehensive commissioning protocol to assess the MRI performance of integrated MRI-linear accelerators, (2) characterize the imaging perfor-

* Corresponding author at: Department of Radiotherapy, University Medical Center Utrecht, Room Q.0S.211, PO Box 85500, 3508 GA Utrecht, the Netherlands.
E-mail address: r.tijssen@umcutrecht.nl (R.H.N. Tijssen).

https://doi.org/10.1016/j.radonc.2018.12.011
0167-8140/

mance of existing 1.5T MR-linac systems in a multi-institutional study, and (3) provide a bench mark data set by making the results as well as the measurement protocols publicly available. To limit the scope of this paper, items related to site planning, system installation, and MR safety are not covered here.

Materials & methods

System overview

All imaging tests were performed on pre-clinical Elekta Unity MR-linac systems (Elekta AB, Stockholm, Sweden) equipped with a Philips Marlin 1.5T MRI scanner (Philips Healthcare, Best, the Netherlands). The MRI component is based on the wide bore 1.5T Ingenia system, but with modifications to make the system compatible with a linear accelerator in perpendicular configuration (Fig. 1). A ring gantry, which holds all the beam generating components, such as the magnetron, waveguide, a standing wave linear accelerator, and the Multi Leaf Collimator (MLC), is positioned around the cryostat. The active shielding of the magnet has been modified to create a torus of near zero magnetic field around the magnet at the location of the sensitive electronic components, waveguide, and the gun of the Linac. The cryostat has been integrated into the Faraday cage to minimize radiofrequency interference of the Linac components on MR signal acquisition. The cryostat and B_0 coils have been modified to minimize beam attenuation, and the gradient coils are physically split, which creates a radiation window of 22 cm at isocenter. The system is equipped with a 2×4 channel radiolucent receive array (coil), with electronic components placed outside the radiation window to minimize attenuation and radiation induced currents that may impact image quality [17–19].

Commissioning protocol

The complete commissioning protocol is listed in Table 1. The table is subdivided into six sections. The first section describes the System Configuration and Connectivity (SCC) checks. Sections 2–5 consist of Quality Control (QC) tests, designed to test the performance of individual subsystems of the MRI scanner. Finally, section 6 includes Quality Assurance (QA) measurements. These assess the overall image quality, thereby testing a combination of hardware components [20], making them suitable for periodic QA.

Where possible, the QC and QA tests are based on the tests described in the guidance documents of the American Association of Physics in Medicine (AAPM) [3], and the American College of Radiology (ACR) [4]. The widespread availability of the ACR phantom facilitates cross-institutional comparison. Some tests, however, are adapted to meet the radiotherapy-specific requirements.

System configuration & connectivity (SCC)

After the general inventory, in which the software configuration and presence of all software options, receiver coils, and other peripherals is checked, the basic functionality of the MR scanner is tested. This test set includes: storing and exporting DICOM images and connectivity to hospital PACS (1.2), functioning of scanner peripherals such as the patient couch (1.3), patient communication system (1.4), and in room camera system (1.5).

Quality Control (QC)

The QC tests are to assess the three subsystems: the static magnetic field (**B_0 field**), the **imaging gradients**, and the **RF fields**. Additionally, **hybrid** specific tests have been designed, which test for interactions between the Linac and MRI components of the system.

For MR-guided systems it is vital that the static magnetic field strength is accurately known, spatially homogeneous, and stable over time, because magnetic field determines the (local) resonance frequency (f_0) of the system and thus the spatial localization. The absolute field strength test (2.1) compares the system specified f_0 with the system calibration values. Monitoring based on the log files may be performed to track long term f_0 drifts (2.2) as well as monitoring of cryogen levels (2.3). The B_0 homogeneity is measured by a dual echo B_0 mapping sequence (2.4) on a 40 cm flood field phantom (Fig. 2a).

A thorough characterization of the imaging gradients is required, as it directly determines the geometric fidelity of the object that is scanned. Test (3.1) checks whether the image orientation as represented by the MRI host and treatment planning system (TPS) agrees with the physical setup in all four orientations (Fig. 2b). The amount of ghosting (3.2) is then measured for two pulse sequences with a high gradient duty cycle to assess the fidelity of the gradient system. The gradient delays and eddy currents are not assessed individually, but instead included in section 6 as part of the sequence specific tests.

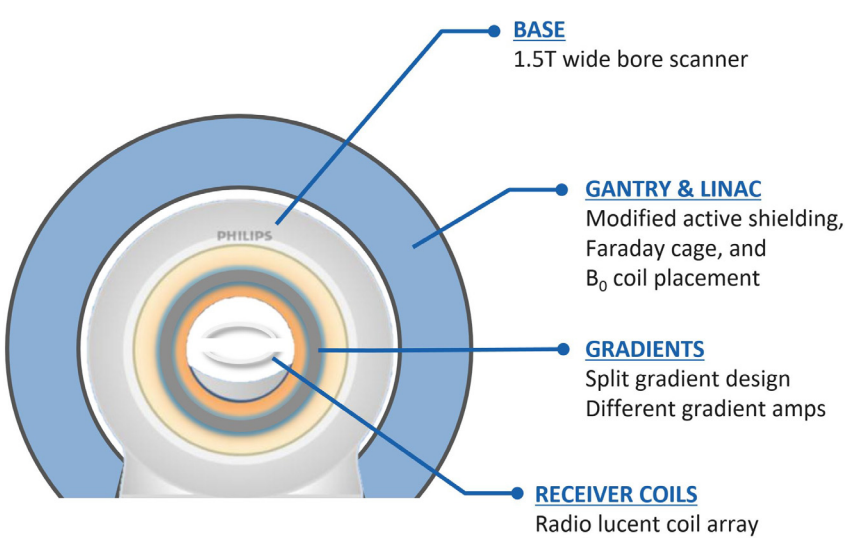

Fig. 1. Overview of the hybrid hardware components that make the MR-linac different compared to normal diagnostic scanners.

Table 1
List of commissioning tests ordered by test type (SCC, QC, and QA).

System configuration and Connectivity (SCC)					
System & connectivity	test#				
general inventory	1.1				
DICOM functionality	1.2				
patient couch	1.3				
patient communication	1.4				
cameras	1.5				
Quality Control (QC)					
B0 field	test#	Field gradients	test#	RF fields	test#
absolute field strength	2.1	Image orientation	3.1	flip angle accuracy	4.1
f0 stability	2.2	ghosting	3.2	spurious noise	4.2
cryogen level	2.3	*gradient delays*[*]	–	receiver coil performance	4.3
B0 homogeneity	2.4	*eddy currents*[*]	–		
HYBRID TESTS	test#	*HYBRID TESTS*	test#	*HYBRID TESTS*	test#
B0 direction	5.1	gradient fidelity	5.3	linac induced RF interference	5.4
gantry dependent B0	5.2			radiation influence	5.5
Quality Assurance (QA)					
General image quality	test#	Sequence specific tests	test#		
PIQT	6.1	signal-to-noise	6.4a		
ACR	6.2	low contrast detectability	6.4b		
FBIRN	6.3	gradient fidelity	6.4c		

[*] Gradient delays and eddy currents not quantified separately, but included in the sequence specific tests.

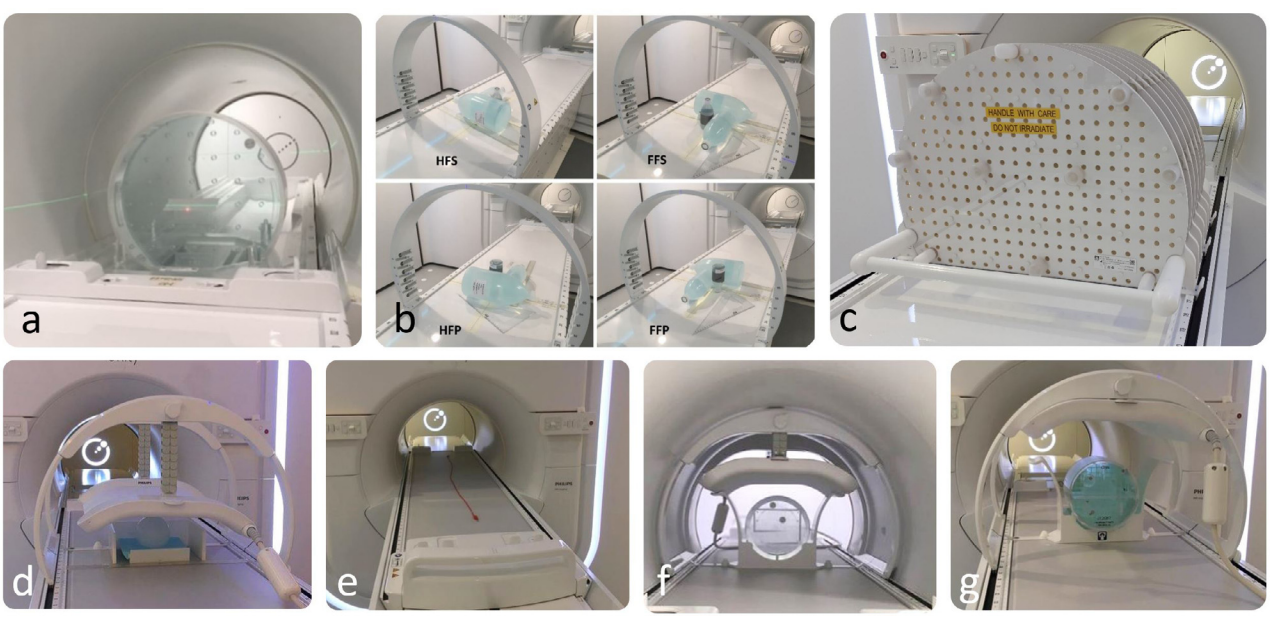

Fig. 2. Phantom setups of various tests in the commissioning protocol. (a) B_0 homogeneity (2.4), (b) image orientation (3.1), (c) gradient fidelity (5.3), (d) flip angle accuracy (4.1), e) spurious noise (4.2), f) PIQT (6.1), and (g) ACR (6.2).

The RF subsystem consists of three tests: flip angle accuracy (4.1), which checks the RF power calibration; spurious noise (4.2), which detects spurious noise caused by external equipment; and coil performance (4.3), which measures the signal to noise and coupling of the RF receive channels.

Hybrid tests are tests that deviate from the standard, diagnostic radiology, QC measurements. These tests are either important from a therapy point of view, or specific to the hardware modifications of the MR-linac. The direction of the main magnetic field (5.1) must be verified as it determines the direction of dose kernel tilt and the electron return effect (ERE). Test (5.2) is designed to measure the B_0 homogeneity as a function of gantry angle. Because the gantry contains large amounts of ferromagnetic material, the gantry can introduce spatially varying offsets to the B_0 field, which could lead to image artifacts. For this test, B_0 maps of a 40 cm cylindrical phantom in transverse orientation are obtained for gantry angles between 0° and 360° degrees with 30° intervals. Test (5.3) characterizes the gradient fidelity of the split gradient system of the MR-linac on a large ($500 \times 375 \times 330\ mm^3$) geometric fidelity phantom provided by Philips. This phantom contains 1932 markers spaced 25 mm × 25 mm × 55 mm apart. The displacements are calculated by subtracting the marker locations found in the MR dataset from the known marker locations (after a rigid registration is performed on the center of the phantom to correct for phantom setup errors). All measurements are performed twice with gradient polarities reversed, to subtract static B_0 inhomogeneity and susceptibility induced distortions from residual gradient errors [21,22]. Finally, the RF interference produced by the Linac is tested.

Noise only scans (i.e., images acquired without RF excitation) are acquired 1) with the Linac turned off, 2) with the magnetron turned on, but without radiation, and 3) with moving MLCs (5.4). Additionally, phantom scans and noise only scans were performed during irradiation of various field sizes to test the effect of pulsed radiation on the receiver coils (5.5).

Quality assurance (QA)

General image quality tests include: the Philips Periodic Image Quality Test (PIQT) (6.1) provided by the vendor, the ACR periodic phantom tests (6.2) [23], and the Functional Biomedical Informatics Research Network (FBIRN) test (6.3) [24]. All are well established tests and performed at many different centers, which facilitates bench marking with other (non MR-linac) systems. The PIQT is acquired to facilitate efficient communication with the vendor. The ACR phantom test has large overlap with the PIQT test and serves as an independent alternative to the PIQT test. The FBIRN test checks the temporal stability of functional and dynamic time-series measurements. The QA measurements during commissioning serve as a baseline measurement for periodic QA that follows after clinical acceptance.

Additional tests (6.4b) are included to assess the specific sequence that is used for treatment guidance. The gradient fidelity test is performed again to include the effects of gradient delays and eddy currents as these were not characterized by separate QC measurements. Contrast and Signal-to-Noise (SNR) are also sequence specific. For this reason the ACR measurement is also repeated here.

Multi-center bench marking

Four MR-linacs were tested at the following institutions: Medical College Wisconsin (MCW), MD-Anderson (MDA), The Netherlands Cancer Institute (NKI), and University Medical Center Utrecht (UMCU). The configuration of these systems was close to the eventual clinical configuration, although a few components were different (i.e., the patient couch, gantry shims, and imaging software release were updated after completion of data collection). Each institute collected a complete commissioning data set, which was then sent to the UMCU for analysis. A detailed set of instructions on how to perform the tests is provided in the Supplementary material (Appendix A). The scan protocols have been made publically available through the Mendeley Data repository.

Results

All systems performed similarly on the standard (diagnostic) imaging QC and QA tests. A summary table of all the test results as well as the detailed ACR results are provided in the Supplementary material (Appendix B). The results for the hybrid tests are described below.

Fig. 3 shows the gantry dependent B_0 homogeneity results (5.2). The B_0 field maps, with and without active shimming, at various gantry angles are shown for two systems. MRL#4 shows an apparent linear field offset that rotates with the gantry angle when no active shimming is performed (top row, panel a). The dependency is largely mitigated after active shimming (top row, panel b). The effect of gantry angle was not observed for MRL#3 (second row), which showed excellent B_0 homogeneity with and without active shimming. Inspection of the peak-to-peak values (panels c and d) shows that the gantry dependent B_0 homogeneity varies between the four systems. MRL#2 and MRL#4 show peak-to-peak values of around 1200 nT without active shimming (left plot), which is reduced to 400 nT when active shimming is performed (right plot). The peak-to-peak values for MRL#3 lie around 400 nT for both measurements (with and without active shimming), indicating

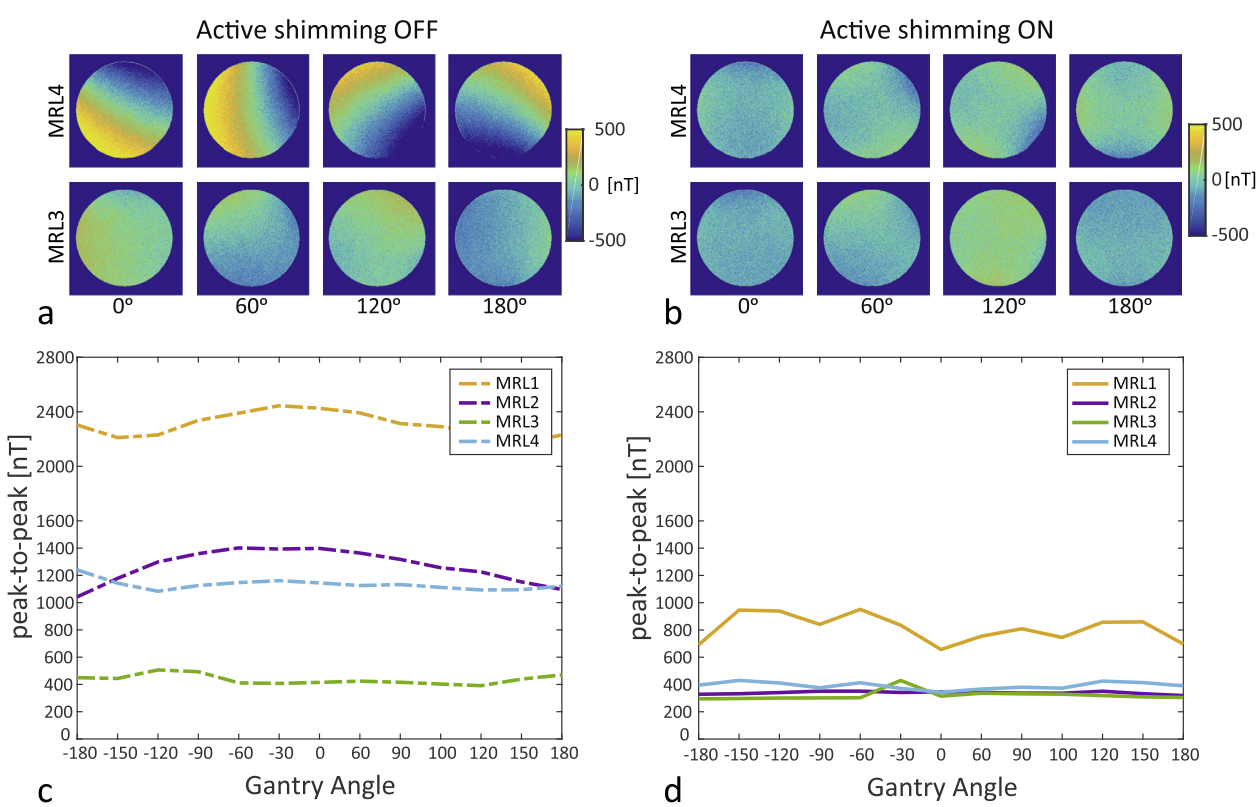

Fig. 3. The effect of gantry angle on the B_0 homogeneity. B_0 field maps at various gantry angles of two MR-linacs (MRL#4 and MRL#3) are shown at the top. The line plots show corresponding peak-to-peak values for all four systems as a function of gantry angle. The left column shows results without active shimming, while the right column shows results with active shimming turned on.

that the passive gantry shims are correctly balanced. MRL#1 shows considerably higher inhomogeneities both with and without active shimming.

Fig. 4 shows the geometric inaccuracies caused by linear and non-linear gradient errors (i.e., after removal of the system B_0 inhomogeneity and susceptibility effects) (5.3). The distortion maps (panel a) show a similar spatial pattern for the × and y gradients (i.e., the LR and AP axes). The total displacement (fourth column, panel a) demonstrates that the error increases with increasing distance to isocenter. Panels b and c show the histogram and cumulative histogram of the displacements within a dynamic spherical volume of 350 mm, respectively. The maximum (99th percentile) displacement values within a DSV of 350 mm were 2.0 mm, 1.7 mm, 1.3 mm, and 1.3 mm for MRL#1, MRL#2, MRL#3, and MRL#4, respectively. Within a DSV of 150 mm, the maximum displacements were 0.7 mm, 0.7 mm, 0.6 mm, and 0.6 mm.

Fig. 5 shows the influence of pulsed radiation on the MR imaging (5.5). From left to right are shown: (1) the image of the phantom, (2) its corresponding k-space, and (3) a noise only k-space, which was acquired in a separate scan without a phantom for better visualization of the effect. The acquisition parameters were set in such a way that the signal bursts all lie on a diagonal line in order to maximize the potential artifacts in image space. The top row (no rad) shows an image and corresponding k-space without radiation, while the second and third row show the results for a $10 \times 10\ cm^2$ and an open $56 \times 22\ cm^2$ field. No detectable image

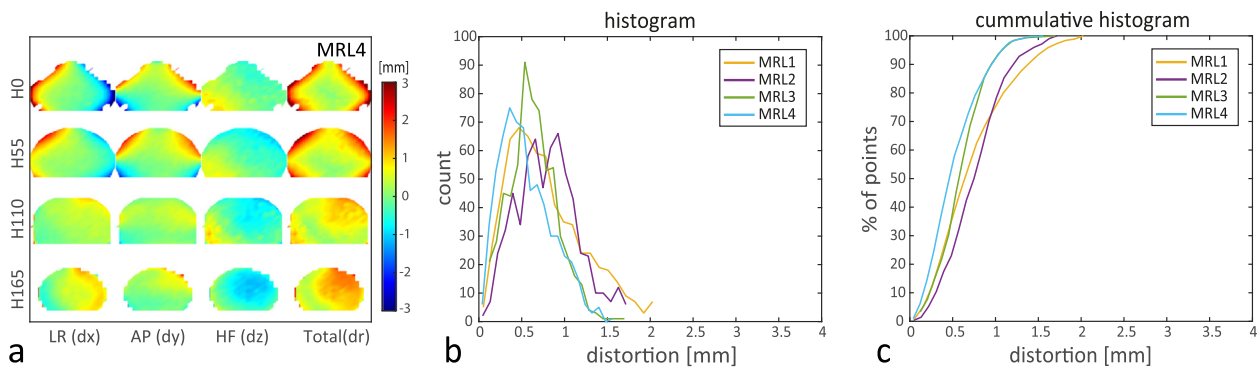

Fig. 4. Geometric fidelity after removal of system B_0 and B_{susc} effects. Panel (a) shows the spatial distribution of the gradient (non-)linearity induced distortion at four different slice locations for MRL#4. Panels (b) and (c) show the histograms and cumulative histograms of the distortions for a DSV of 350 mm.

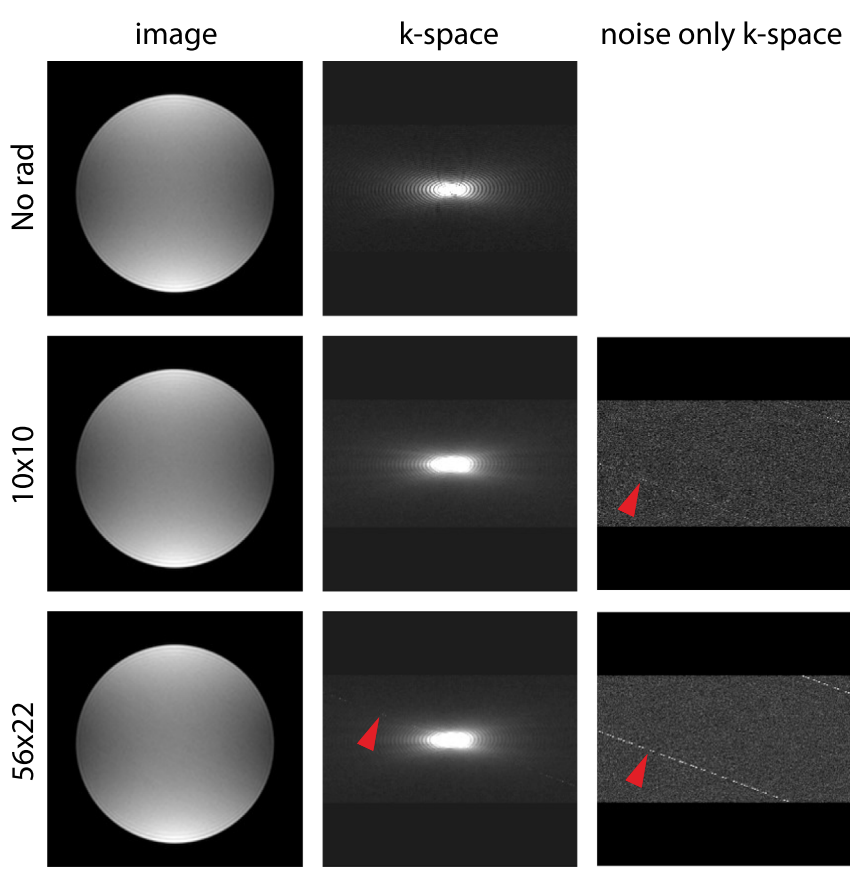

Fig. 5. Radiation influence on MRL#4. The effects in image space and k-space are shown as well as the effect in k-space when a noise-only (i.e., no RF excitation) scan is performed. The latter is used for quantification of the signal bursts.

artifacts were observed when a $10 \times 10\ cm^2$ field was irradiated during imaging and no spikes in k-space were observed. Only the noise acquisition revealed radiation induced spikes in k-space (third column, second row). When data are acquired during radiation with the $56 \times 22\ cm^2$ field a diagonal line of signal bursts is more prominent and visible in both k-spaces. A very faint form of structured noise can be observed in the image, when this diagonal crosses the center of k-space in the dynamically acquired data. The noise only analysis showed that the average intensity of the spikes was approximately double compared to the $10 \times 10\ cm^2$ field size data. Finally, separate RF interference tests, which were designed to detect RF interference by the Linac components, showed no spurious noise when the magnetron was turned on, but no radiation was delivered (4.2 and 5.4, data not shown).

Discussion

The proposed MRI commissioning protocol was designed to provide a practical set of measurements that covers all the subsystems of a hybrid MRI-Linac device. To date, little data has been published on the imaging performance of MR-linac systems, and no formal guidelines exist. Therefore, the current work does not include tolerances on the measurements that were performed. Recently, several working groups within the AAPM, IPEM, and NCS have started to develop formal guidelines on the use of MRI in radiotherapy. Until these guidelines are published this study will provide valuable bench mark data for users of the Unity system and other MR-linac designs [15,25].

Our results indicate that the proposed protocol is sensitive enough to detect variability in performance between the systems on certain hybrid specific tests. The most noticeable differences were observed in the gantry dependent B_0 test (5.2). Whereas one system did not demonstrate any gantry angle dependency, two systems (MRL#2 and MRL#4) showed a clear dependency without active shimming, while another system (MRL#1) showed increased inhomogeneities, even when active shimming was performed. Communication with the vendor revealed that the static shim configuration of these prototypes was different as three of the four systems did not have the adequate shim magnets in place. Following these results corrective actions were scheduled, such that all systems will have a gantry induced peak-to-peak inhomogeneity of less than 500 nT, corresponding to 0.3 ppm.

All four systems demonstrated maximum (99th percentile) displacements of 2 mm or less within a DSV of 350 mm. This is comparable to the 1.88 mm reported for the ViewRay MRIdian system [11] and within vendor specifications. The cumulative histogram in Fig. 4c appears to indicate slight differences in performance between the systems. However, as the accuracy and precision of the measurement is not determined yet, it is unknown whether the differences between the systems are significant.

The pulsed irradiation induced signal bursts in k-space have minimal effect on the image quality (Fig. 5) and were not observed when a $10 \times 10\ cm^2$ field was used. For this reason we believe this effect to be clinically irrelevant for this system. It is therefore not likely that this test will be performed periodically to test image quality. Nevertheless, the fact that the diagonal lines of signal bursts observed in the noise only k-spaces are straight demonstrates that the Linac pulses are in sync with the MRI acquisition, which indicates that the timing is stable for both systems. The measurement could therefore find its use as a diagnostic test when the timing performance of either system is questioned.

Besides radiation therapy specific tests (e.g., geometric accuracy), a significant portion of the commissioning protocol includes tests that are standard (radiological) QC and QA tests. Overall, the performance of the systems was highly comparable for these tests (Supplementary material, Appendix B) and on par with 1.5T diagnostic scanners (Table B2). The comparable performance on tests like the flip angle accuracy (4.1) is promising for applications such as quantitative imaging. However, a more in depth investigation into the accuracy and reproducibility of quantitative imaging methods is still needed before such studies can be conducted.

This work has some limitations. As mentioned above, no separate tests were included that characterize the dynamic gradient behavior, because these test often require specialized equipment in the form of field probes [26], or require assistance of MR vendor service personnel. Eddy currents and gradient delays can, however, have an effect on geometric fidelity and quantitative measures like T2 mapping and DWI. Image based methods have been proposed, which may provide a practical alternative [27–29]. We are currently investigating the suitability of such an approach.

The MR-MV alignment (i.e., the alignment of the imaging and irradiation isocenter) was not included in this commissioning set. Instead, this specific test was allocated to the Linac commissioning. It should, however, be stressed that an independent check of the MR-MV alignment is an essential check for the medical physicist to perform as any error would result in a population wide geometrical bias. When performing such a measurement one should take care that the phantom material is chosen to match the susceptibility of the MR visible solution to minimize susceptibility induced distortions. The readout bandwidth should be high and one could consider acquiring a data set with opposite readout polarities, similar to the gradient fidelity checks (5.3).

A comprehensive commissioning protocol was developed for the MRI component of the 1.5T MRI-Linac and tested on four different systems. Apart from known radiological QC and QA tests, the protocol includes tests that are specific to the MR-linac hardware. Although the four systems showed excellent agreement on most tests, the protocol was able to pick up differences in some of the hybrid specific tests. Until formal guidelines and tolerances are defined these multi-center results provide a bench mark data set for future MR-linac installations.

Conflicts of interest

The University Medical Center Utrecht, Medical College of Wisconsin, Sunnybrook Health Sciences Centre, Christie NHS Foundation Trust, Royal Marsden Hospital NHS Foundation Trust, MD Anderson Cancer Center, and Netherlands Cancer Institute are members of the Elekta MR-linac Consortium, which aims to coordinate international collaborative research relating to the Elekta Unity (MR-linac). Elekta and Philips are commercial partners within the Consortium. Elekta financially supports consortium member institutions with research funding and travel costs for Consortium meetings.

Acknowledgement

This research was supported by a grant from the Dutch Cancer Society (grant number: Alp-H1 UU 2015-8048) to J.J.W. Lagendijk

Appendix A. Supplementary data

Supplementary data to this article can be found online at https://doi.org/10.1016/j.radonc.2018.12.011.

References

[1] Lagendijk JJW, Bakker CJG. MRI guided radiotherapy: a MRI based linear accelerator. ESTRO 2000;19:S1–S255. Istanbul.
[2] Lagendijk JJ, Raaymakers BW, Raaijmakers AJ, Overweg J, Brown KJ, Kerkhof EM, et al. MRI/linac integration. Radiother Oncol 2008;86:25–9.

[3] Jackson EF, Bronskill MJ, Drost DJ, Och J, Pooley RA, Sobol WT, et al. AAPM Report MR TG-1: Acceptance Testing and Quality Assurance Procedures for Magnetic Resonance Imaging Facilities; 2010.
[4] Price R, Allison J, Clarke G, Dennis M, Hendrick RE, Keener C, et al. Magnetic resonance imaging quality control manual. American College of Radiology; 2015.
[5] Kapanen M, Collan J, Beule A, Seppala T, Saarilahti K, Tenhunen M. Commissioning of MRI-only based treatment planning procedure for external beam radiotherapy of prostate. Magn Reson Med 2013;70:127–35.
[6] Liney GP, Owen SC, Beaumont AK, Lazar VR, Manton DJ, Beavis AW. Commissioning of a new wide-bore MRI scanner for radiotherapy planning of head and neck cancer. Br J Radiol 2013;86:20130150.
[7] Xing A, Holloway L, Arumugam S. Commissioning and quality control of a dedicated wide bore 3T MRI simulator for radiotherapy planning. Int J Cancer Therapy Oncol 2016;4:421.
[8] Paulson ES, Erickson B, Schultz C, Allen Li X. Comprehensive MRI simulation methodology using a dedicated MRI scanner in radiation oncology for external beam radiation treatment planning. Med Phys 2015;42:28–39.
[9] Glide-Hurst CK, Wen N, Hearshen D, Kim J, Pantelic M, Zhao B, et al. Initial clinical experience with a radiation oncology dedicated open 1.0T MR-simulation. J Appl Clin Med Phys 2015;16:5201.
[10] Saenz DL, Yan Y, Christensen N, Henzler MA, Forrest LJ, Bayouth JE, et al. Characterization of a 0.35T MR system for phantom image quality stability and in vivo assessment of motion quantification. J Appl Clin Med Phys 2015;16:30–40.
[11] Ginn JS, Agazaryan N, Cao M, Baharom U, Low DA, Yang Y, et al. Characterization of spatial distortion in a 0.35 T MRI-guided radiotherapy system. Phys Med Biol 2017;62:4525–40.
[12] Wang J, Yung J, Kadbi M, Hwang K, Ding Y, Ibbott GS. Assessment of image quality and scatter and leakage radiation of an integrated MR-LINAC system. Med Phys 2018;45:1204–9.
[13] Mutic S, Dempsey JF. The ViewRay system: magnetic resonance-guided and controlled radiotherapy. Semin Radiat Oncol 2014;24:196–9.
[14] Keall PJ, Barton M, Crozier S. The Australian magnetic resonance imaging-linac program. Semin Radiat Oncol 2014;24:203–6.
[15] Fallone BG. The rotating biplanar linac-magnetic resonance imaging system. Semin Radiat Oncol 2014;24:200–2.
[16] Raaymakers BW, Lagendijk JJ, Overweg J, Kok JG, Raaijmakers AJ, Kerkhof EM, et al. Integrating a 1.5 T MRI scanner with a 6 MV accelerator: proof of concept. Physics in. Med Biol 2009;54:N229–37.
[17] Burke B, Fallone BG, Rathee S. Radiation induced currents in MRI RF coils: application to linac/MRI integration. Phys Med Biol 2010;55:735–46.
[18] Burke B, Wachowicz K, Fallone BG, Rathee S. Effect of radiation induced current on the quality of MR images in an integrated linac-MR system. Med Phys 2012;39:6139–47.
[19] Hoogcarspel SJ, Zijlema SE, Tijssen RHN, Kerkmeijer LGW, Jurgenliemk-Schulz IM, Lagendijk JJW, et al. Characterization of the first RF coil dedicated to 1.5 T MR guided radiotherapy. Phys Med Biol 2018;63:025014.
[20] Thomadsen B. Quality management in medical physics: general concepts. AAPM 2004. Pittsburg, PA.
[21] Moerland MA, Beersma R, Bhagwandien R, Wijrdeman HK, Bakker CJ. Analysis and correction of geometric distortions in 1.5 T magnetic resonance images for use in radiotherapy treatment planning. Phys Med Biol 1995;40:1651–4.
[22] Stanescu T, Wachowicz K, Jaffray DA. Characterization of tissue magnetic susceptibility-induced distortions for MRIgRT. Med Phys 2012;39:7185–93.
[23] Large Phantom Guidance. American College of Radiology; 2018.
[24] Friedman L, Glover GH. Report on a multicenter fMRI quality assurance protocol. J Magn Reson Imaging 2006;23:827–39.
[25] Keall PJ, Barton M, Crozier S. The Australian magnetic resonance imaging-linac program. Semin Radiat Oncol 2014;24:203–6.
[26] Vannesjo SJ, Haeberlin M, Kasper L, Pavan M, Wilm BJ, Barmet C, et al. Gradient system characterization by impulse response measurements with a dynamic field camera. Magn Reson Med 2013;69:583–93.
[27] Duyn JH, Yang Y, Frank JA, van der Veen JW. Simple correction method for k-space trajectory deviations in MRI. J Magn Reson 1998;132:150–3.
[28] Brodsky EK, Klaers JL, Samsonov AA, Kijowski R, Block WF. Rapid measurement and correction of phase errors from B0 eddy currents: impact on image quality for non-Cartesian imaging. Magn Reson Med 2013;69:509–15.
[29] Jang H, McMillan AB. A rapid and robust gradient measurement technique using dynamic single-point imaging. Magn Reson Med 2017;78:950–62.